Cislunar Multiscale Dynamics and Implications for SSA

Aaron J. Rosengren
University of California San Diego, La Jolla, CA, United States

ABSTRACT

To enable and protect the critical elements of the combined commercial, civil, and military command, control, communications, computer, intelligence, surveillance, and reconnaissance (C4ISR) infrastructure in the cislunar space beyond the geosynchronous belt (xGEO) requires a more fundamental understanding of the multi-timescale dynamics in this regime. The nonlinear astrodynamics in xGEO, encompassing secular, resonant, chaotic, close-encounter, and manifold dynamics, is dramatically different than the weakly perturbed Keplerian approach used for over a half century for the detection and tracking of objects near Earth. To date only the relatively short timescale dynamics of libration-point orbits (LPOs) and and their associated invariant manifolds have been partially coupled with the cardinal questions and problems posed by cislunar space situational awareness (SSA). Here, we review the foundational dynamics in the entire cislunar regime, including lunar mean-motion resonances (MMRs) and secular resonances, which have hitherto not been rigorously investigated, to holistically improve SSA capabilities beyond the traditional geocentric domains. We provide dynamical cartographies using an xGEO orbit parameterization applicable throughout the entire cislunar region, which can be leveraged for surveillance design strategies.

1. INTRODUCTION

As new transportation, communication, and logistic infrastructures are being planned and developed for cislunar space in the Earth-Moon system, the need for improved space situational/domain awareness (SSA/SDA) beyond the geostationary belt (xGEO) becomes paramount [1]. Cislunar space refers to the orbital regimes about the Earth out to and including the region around the surface of the Moon (Fig. 1). To study the great diversity of trajectories in cislunar space, nicely summarized in [2], requires employing a wide variety of dynamical models. Whereas circumterrestrial and circumlunar orbits are largely governed by the perturbed two-body problem [3], in which the effects of the non-spherical gravity field and third-body perturbations on Earth or Moon satellites are often treated in a Hamiltonian formulation (see, e.g., [4–6]), all other cislunar trajectories, including lunar transfers and libration-point orbits (LPOs), are specific applications of the gravitational N-body problem [7, 8]. The simplest way to model trans-lunar trajectories is with the method of patched conics, whereby the Moon's sphere of influence (SOI) or Hill sphere separates selenocentric from geocentric motions (Fig. 1, *left panel*). More realistically, however, trans-lunar trajectories are governed by the restricted three-body problem (R3BP), in which the spacecraft of negligible mass is simultaneously affected by the terrestrial and lunar gravitational forces. This framework efficiently captures Earth-Moon orbital transfers [9, 10], models the regions of the Lagrange equilibrium points shown in Fig. 1 (*right panel*) [11], and has generally been the most studied mathematical formulation of motion in cislunar space [12–17].

Developing and maintaining a SOC for cislunar space beyond GEO will require significant improvements in our knowledge of the way objects behave in this complicated multi-body environment over orbital, decadal, and even centennial timescales. However, most studies to date have mostly focused on the orbital timescales of LPOs within the framework of the planar, circular, and restricted three-body problem (PCR3BP) [7, 19] or a hierarchy of more realistic, and more complicated, dynamical models [20–22], e.g., the elliptical orbit of the Moon, three-dimensional motion of the satellite, and, more recently, on the fourth-body effects from the Sun (i.e., bi-circular and restricted Hill problems, respectively designated BR4BP and RH4BP). Of the myriad of trajectories uncovered by these fundamental mathematical models, the distant retrograde orbits [16, 23–29] and near-rectilinear halo orbits [21, 30–36] have assumed a special significance. DROs, which are stable geocentric orbits that resemble large quasi-elliptical retrograde orbits around the Moon in the rotating frame, have been proposed as parking orbits for interplanetary missions [26, 37] and for the unfunded Asteroid Redirect Mission [38, 39]. Halo orbits about L_1 and L_2 have been proposed for payloads supporting lunar exploration and communication [34, 36, 40], including the Lunar Gateway [35, 41], as well as a

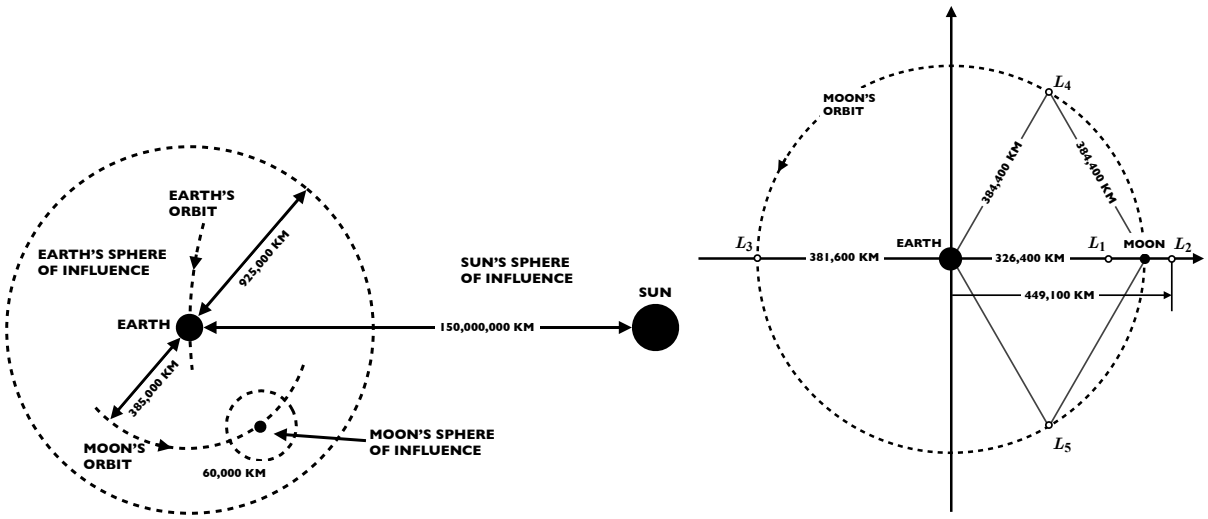

Fig. 1: Approximate sphere of influence or Hill sphere of the Earth, Moon, and Sun (*left*) and the locations of the five Lagrange points in the Earth-Moon system (*right*) [18]. The lunar Hill sphere is the region between diametrically opposite collinear Lagrange points L_1 and L_2, in which the motion of the satellite is dominated by the attraction of the Moon. (Not to scale.)

parking orbit for the efficient insertion of satellites into low-Earth orbits (LEOs) [42]. The later scenario is particularly ominous for SDA as payloads could be deployed into a multitude of orbits from above, responsively and clandestinely, without the indications and warnings normally associated with a new foreign launch. There is, furthermore, a dynamical plethora of Earth-bound trajectories beyond the geosynchronous region that must be more deeply understood to enable robust cislunar SSA [43–45].

For the investigation of the Earth's magnetosphere and the interplanetary space outside of it, satellites with orbits of high eccentricity, large semi-major axis, and multi-day period are often used [46–51]. Under the influence of the Moon and the Sun, a highly eccentric orbit of a deep space probe can become nearly circular or a nearly circular orbit might become eccentric, while orbital inclination may also exhibit large shifts [52–54]. NASA's eccentric Orbiting Geophysical Observatory (1964-054A), colloquially referred to as EGO, with a semi-major axis of 12.7 Earth radii and an eccentricity of 0.918, is particularly interesting as it only reentered in August 2020, in contrast to earlier predictions that indicated a lifetime of only 16 years [52]. A more modern example is ESA's International Gamma-Ray Astrophysics Laboratory (INTEGRAL) satellite (72-hour period with $e \sim 0.9$), which despite the longevity of its original operational orbit (orbital lifetime greater than two centuries), will now come down in 2029 as its orbit was modified via a series of four thruster burns [55]. Finally, for orbits where the semi-major axis is a substantial fraction of the Moon's, several orbital revolutions may be sufficient to lower the perigee height below the Earth if an unfavorable orbital configuration is chosen [44]. Among the first and perhaps the most interesting of this class of very distant, highly eccentric satellites was the Soviet space probe, Luna 3 (1959 Theta 1), which circumnavigated the Moon (passing through its SOI) and returning to the Earth on a new elliptical trajectory. Luna 3 twice suffered close approaches with the Moon, and despite having an initial perigee height outside of the GEO belt, after only 11 revolutions it plummeted to Earth [45, 56]. The Interstellar Boundary Explorer (IBEX) and the Transiting Exoplanet Survey Satellite (TESS), two modern Luna-3 like orbits, are distinguished by their high apogee distances and lunar mean-motion resonance (MMR) phasing [51, 57]. IBEX (2008-051A), with its nominal mission lasting only 2 years, had to change its operational orbit for its extended mission to avoid violating altitude and eclipse mission constraints. Its nominal orbit turned out to be chaotic and unpredictable beyond 2.5 years, as a result of significant lunar perturbations, and IBEX was subsequently placed in a novel 3:1 MMR with the Moon ($P_M/3$). Following suit, TESS (2018-038A) orbits in a 2:1 lunar MMR ($P_M/2$), which was established using a lunar swing-by maneuver [58].

While MMRs (commensurabilities of orbital periods) constitute one of the most important and far-reaching aspects of dynamical astronomy [59–61], they have remained seriously underrated in Earth-satellite dynamics in part because

the orbits of most traditional satellites are too low to be affected by mean-motion commensurabilities. "What are the *Kirkwood gaps* of cislunar space?" This question is of great current interest for mission planners now that we are locating our space-based assets, such as the IBEX and TESS, in predominant lunar MMRs that have hitherto only been treated in piecemeal. A many-sided and detailed investigation of the resonant structure of xGEO space, aside from its own particular significance, is of prime importance for SSA beyond GEO as such resonances significantly affect the global structure of orbital phase space. Furthermore, the manifolds emanating from unstable first-order MMRs, which can enable rapid dynamical transfers, have been largely underappreciated and unexplored in the planetary-science context [62] and only recently investigated in the astrodynamics of icy-world missions [63–65]. These voids in fundamental knowledge is a central motivation of this work.

The multi-timescale dynamics of geocentric and selenocentric orbits (governed by the perturbed two-body problem) and libration-point orbits (governed by the restricted three-body problem) can be treated in a holistic fashion using state-of-the-art dynamical stability metrics [66], such as the fast-Lyapunov indicator (FLI) and Mean Exponential Growth factor of Nearby Orbits (MEGNO) method. Here, we provide a dynamical cartography of the entire cislunar region, including the "cone of shame" or lunar exclusion zone, using the familiar and intuitive concept of geocentric orbital elements, which we show herein can often be well posed for various aspects of importance for SSA. These atlases cover the wide range of orbital phase space relevant to both historic and current cislunar missions launched by the US (e.g., AMPTE, Chandra X-ray Observatory, several EXPLORER series satellites, ARTEMIS), Europe (e.g., XMM-Newton, Cluster II), Russia (e.g., Prognoz, Spektr-R, Astron), as well as the significant future xGEO missions scheduled or proposed by over a dozen nations or organizations to be launched in this decade. The topology of the uncovered structures can enable observers to decide where and when data should be obtained in future campaigns, for example, by providing stringent constraints through stability analysis of the existing and predicted orbital architectures. For the numerical simulations, we use the `IAS15` integrator [67, 68], available within the public-domain `REBOUND` software package [69], as well as the regularized formulations in the `THALASSA` Earth-satellite orbit propagation tool [45, 70], which is assessable through a GitLab repository.[1] These integrators can accurately handle orbital evolution that is highly sensitive to initial conditions, including close approaches and resonances.

2. XGEO ORBIT PARAMETERIZATIONS

The simplest model that approximates the motion of real objects in cislunar space is the PCR3BP. This idealized mathematical model consists of a massless test particle (TP), and two massive bodies (e.g., Earth and Moon) moving in circular orbits about their common center of mass, with all bodies moving in the same plane. Unlike the two-body problem, however, which has a closed-form geometric and analytical description of the motion in terms of the conical orbital elements, the three-body problem possesses only one constant of motion—the Jacobi integral. The Earth-Moon Lagrange points are the five stationary solutions or equilibria in the PCR3BP, where L_1, L_2, and L_3 lie along a line joining the Earth and Moon, and L_4 and L_5 form equilateral triangles with them (Fig. 1, *right panel*). The Moon's Hill sphere is the region between diametrically opposite collinear Lagrange points L_1 and L_2, in which the motion of the TP is dominated by the attraction of the Moon. It is precisely within the lunar Hill sphere that the concept of geocentric orbital elements become ill-posed and a switch to selenocentric elements must be adopted.

Associated with the unstable collinear Lagrange points, or their dynamical extensions to periodic or quasi-periodic orbits, are stable and unstable manifolds, phase-space structures that asymptotically approach or depart the Lagrange points (or their dynamical extensions). The periodic orbits most often treated in the literature—the Lyapunov orbits—reside in the bottlenecks that partition the interior and exterior Hill's regions (see, e.g., [7, 8, 19, 22, 71]). The underlying space-manifold structures that connect the Lagrange points to other periodic orbits and resonances allow the classification of distinctly different types of global motions of the PCR3BP in terms of their relation to the equilibrium points, including transition between the two realms, scattering, temporary capture, and collision.

The unquestionable merit of the PCR3BP model cannot be overstated as it provides the underlying dynamical skeleton (i.e., the Lagrange points and their associated phase-space structures) that organizes and governs how all the possible orbital behaviors are related. The transition to a full ephemeris model, including solar and other gravitational perturbations and solar-radiation pressure (SRP), introduces additional nuances that have only been treated in piecemeal for isolated trajectories. To establish and maintain a cislunar space catalog, however, requires a more holistic and global understanding of such realistic dynamics over orbital and longer timescales. The catalog-maintenance problem also

[1] URL: `https://gitlab.com/souvlaki/thalassa`.

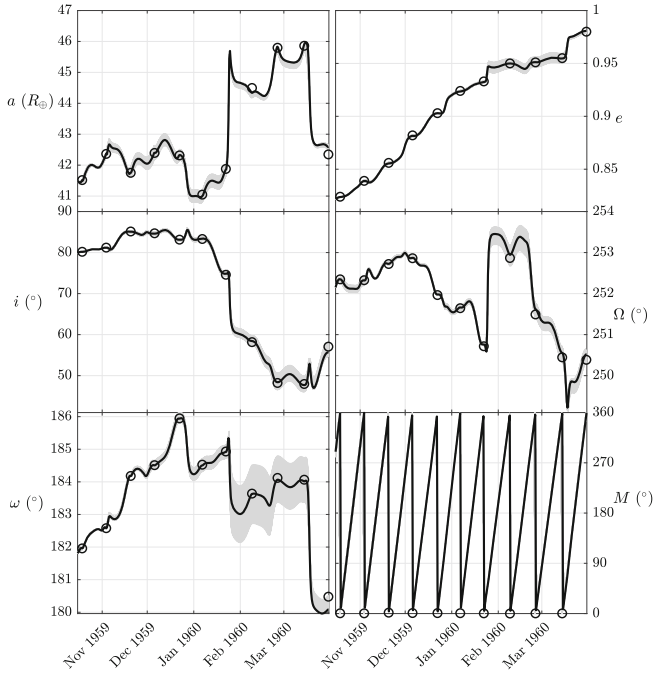

Fig. 2: Evolution of the geocentric ecliptic orbital elements of Luna 3 adapting the restricted four-body problem (R4BP) ephemeris model in `THALASSA`. [45]. *Black lines* correspond to the numerical propagations of the nominal initial conditions given by [72] with its recorded orbital-history given by *circles*, while *grey lines* corresponds to ensemble propagations to account for orbit uncertainties.

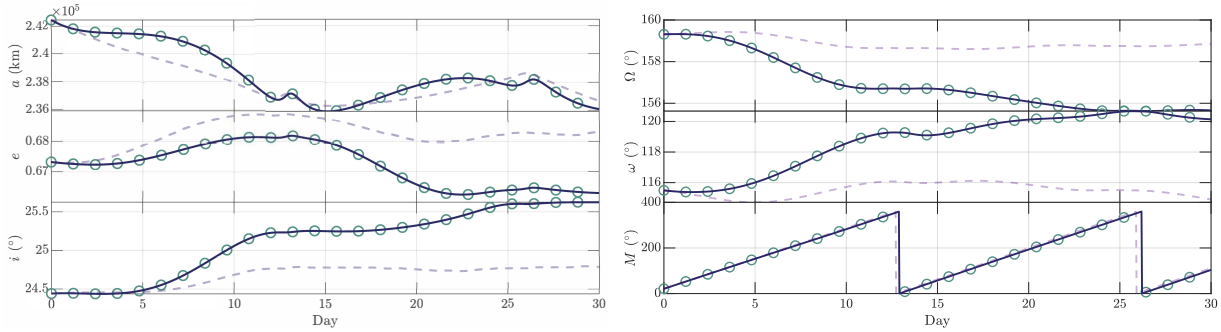

Fig. 3: Simulation of the orbital evolution of TESS adapting a dynamical model in `REBOUND` [67–69] that contains both the Moon and Sun as perturbers (*blue curve*) or only the Moon (*purple dashed curve*). The ephemeris, obtained from the JPL Horizons web-service, is overlaid as *green circle*.

---

necessitates the development of an xGEO orbit parameterization applicable throughout the cislunar region. While "the ubiquitous two-line element (TLE) will no longer suffice" [15], we showcase herein the overlooked utility of the classical osculating-element representation for the cislunar SSA context.

As an interesting historical example, Fig. 2 shows the strongly perturbed, multiple close-encounter dynamics of Luna 3, described in §1. Luna 3 demonstrated how the passage of a spacecraft through the Moon's Hill sphere can be exploited to produce orbits of a very different kind; such swing-by maneuvers were used by both IBEX and TESS to establish their current operational orbits. For TESS, we also consider a 30-day propagation of its resonant orbit, shown in Fig. 3, under both the restricted Earth-Moon-Sun-satellite and Earth-Moon-satellite ephemeris models. We note that for both Luna 3 and TESS, only the more realistic 4BP physical model was able to reproduce the ephemerides, indicating that simplified phenomenological models (e.g., the PCR3BP) are not well suited for cislunar SSA. It is, nevertheless, quite

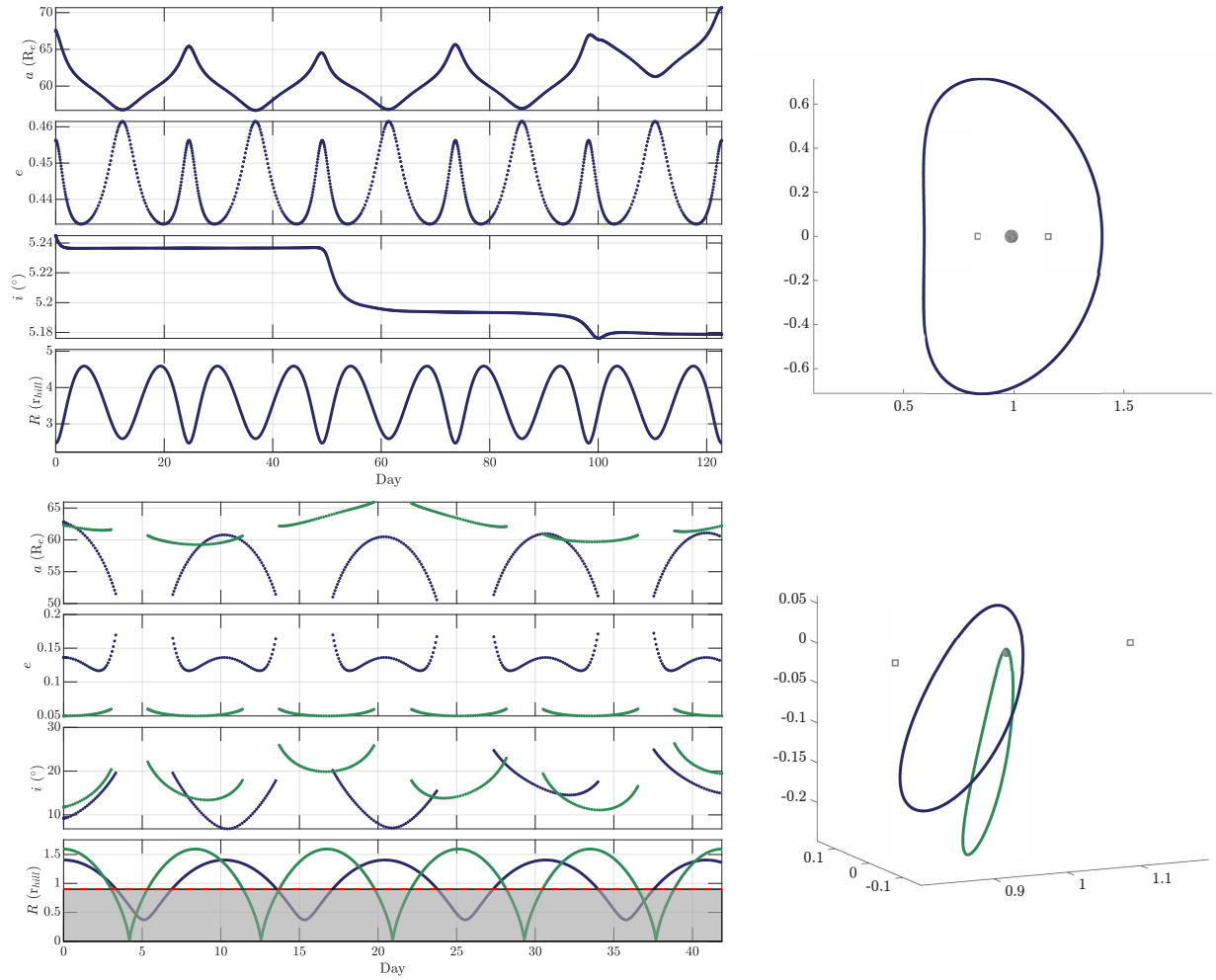

Fig. 4: Geocentric osculating elements (a, e, i) for select LPOs, along with the lunar-close-approach distance. Note that the conversion from the Earth-Moon rotating frame coordinates to inertial ecliptic elements is not made during the passage through the lunar Hill sphere (a threshold of 0.9 r_{hill} was used). The selenocentric orbital elements are not shown here.

---

the mistaken view to believe that the age-old concept of orbital elements has no real merit for the xGEO regime [15].

We note that the concept of geocentric elements (as physically-insightful parameters) do lose their precise meaning upon entering the lunar Hill sphere, but it is at that dynamical constraint where a switch to selenocentric elements can be made. The NRHO of the planed Lunar Gateway, for instance, will bring the station within 3,000 km of the lunar north pole at closest approach and as far as 70,000 km over the lunar south pole. Bearing the aforementioned caveats in mind, one would expect it to have a well defined osculating set of geocentric elements for the majority of its nearly 7-day orbit. DROs, on the other hand, are expected to be generally well behaved in their entire orbital element time histories [28]; with the exception of the vary tightly bound members of this family. Fig. 4 shows some demonstrative results on the use of piecewise osculating elements, geocentric or selenocentric, as the physical picture dictates, for LPOs. A further illustration is provided by the projection of segments of the trajectories of the NASA ARTEMIS spacecrafts [71] (designed in the Earth-Moon rotating frame) into both the Earth and Moon inertial frames, respectively (Fig. 5). Within the bounded motions, the geocentric orbital elements would be generally well behaved, whereas the lunar elements would occasionally lose physical meaning. We should note that García Yárnoz et al. [31] followed in a similar vein by projecting the space-manifolds into orbital element space (a, e, i) and defined reachability sets for asteroid retrieval.

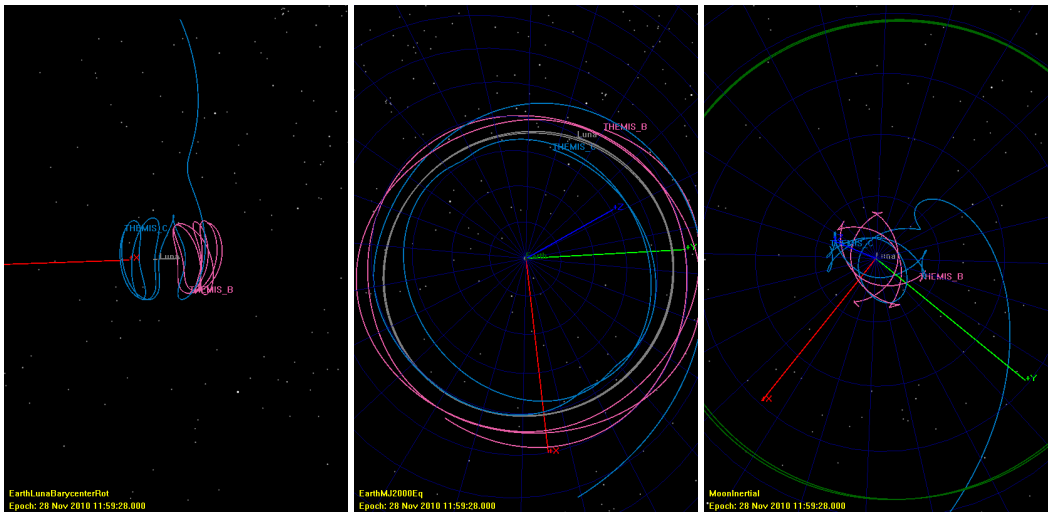

Fig. 5: Segments of the trajectories of NASA ARTEMIS spacecrafts [71] in the Earth-Moon rotating frame (*left*), Earth inertial frame (*middle*), and Moon inertial frame (*right*), using the General Mission Analysis Tool (GMAT) software of NASA's Goddard Space Flight Center (GSFC).

Recent developments, furthermore, have extended the SGP4 capabilities for deep-space modeling [73]. There are roughly 75 multi-day satellites in the SOC with the following orbital characteristics:

- 1501 min $<$ period $<$ 7484 min
- 0.003 $<$ eccentricity $<$ 0.9098
- 0.1 deg $<$ inclination $<$ 133.8 deg
- 685 km $<$ perigee $<$ 50,034 km
- 37,142 km $<$ apogee $<$ 209,209 km

For these Earth-bound satellites, the new SGP4-XP prediction model, developed by Hoots, was found to yield a one to two orders of magnitude improvement over SGP4 with comparable run times. Surprisingly, it could even handle extreme cislunar orbits, such as TESS and a temporary captured (heliocentric) surveyor mission Centaur rocket body, thereby showcasing the applicability of the classical osculating-element and modified TLE representations for the cislunar SSA context, in stark contrast to the dogmatic statements made in [1].

3. CARTOGRAPHIES FOR CISLUNAR SURVEILLANCE AND CATALOG MAINTENANCE

Cislunar SSA captures not only an unprecedented 1000+ volumetric expansion but also a dramatic change in the fundamental motion of RSOs [1]. Orbital motion in the cislunar realm beyond GEO is described to a reasonable accuracy by the restricted three-body problem and remote sensing, regardless of the phenomenology, must accommodate the complex dynamics in this domain. The unequivocal consensus is that the orbital motion of a satellite in this environment is highly chaotic, subject to rapid changes and unexpected developments in its trajectory. These challenges are greatly intensified when one considers the complexity of remotely tracking multiple uncooperative RSOs, each capable of frequent and abrupt changes in their orbital patterns through maneuvers and other events.

The dynamical classification of trajectories can be investigated numerically using the broad family of Lyapunov and affiliated indicators [66]. Many first-order stability metrics, including the fast-Lyapunov indicator (FLI) [74] and Mean Exponential Growth factor of Nearby Orbits (MEGNO) method [75], are based on the propagation of the variational system and on the monitoring of the stretching of the tangent vector with time [66]. Writing the n-dimensional dynamical system in first-order autonomous form, $\dot{x} = f(x)$, where $x \in \mathbb{R}^n$ and $f : \mathbb{R}^n \to \mathbb{R}^n$ represents the vector

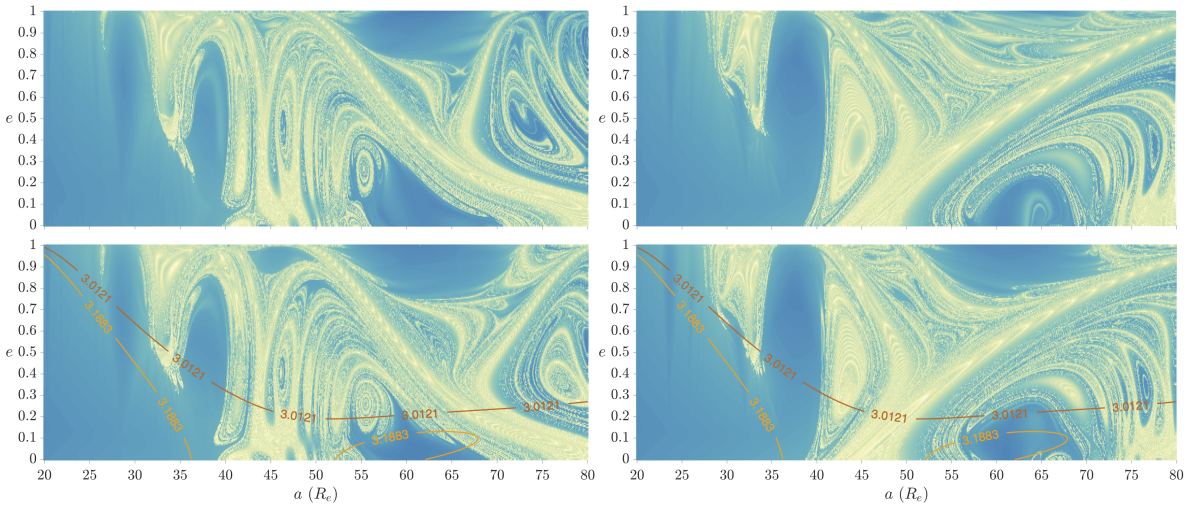

Fig. 6: Space-manifold maps of the region between xGEO and to just beyond the semi-major axis of L_2, adopting a dynamical model that contains the Sun and Moon as perturbers (*top*) or only the moon (*bottom*). The map samples over a dense grid of initial values of (a,e), where the initial inclination i, argument of perihelion ω, and longitude of ascending node Ω are set equal to that of the Moon at the initial epoch 1 Jan. 2021. The initial mean anomaly of the test particles is set to 60° ahead of the Moon in its orbit to reflect the L_4 (*left*) or beyond for the L_5 (*right*) configuration. Orbits located on stable manifolds appear with a lighter color, while darker regions correspond to trajectories off of them. Three-body energy curves (Jacobi contours) are superimposed on the maps.

---

field, the variational system in $\mathbb{R}^{2n}$ can be stated as

$$\dot{x} = f(x), \quad \dot{w} = \left(\frac{\partial f(x)}{\partial x}\right) w,$$

where $w \in \mathbb{R}^n$ stands for the deviation (or tangent) vector. The FLI follows from the variational system and enables the discrimination between ordered and chaotic motions. The indicator at time t is defined by:

$$\mathrm{FLI}(x(0),t) \equiv \sup_{\tau \leq t} \log ||w(\tau)||.$$

FLI increases almost linearly with time for chaotic orbits, and approximately logarithmically for regular motions. When computed for very short timescales the FLI can capture and reveal space manifolds [62, 76], whose short-time dynamics leads to a complicated array of behaviors. The MEGNO is two times the difference between the FLI and its time-average and has been adopted in the `REBOUND` software package [67–69]. The computation of the FLI or MEGNO on two-dimensional grids of initial conditions provides a clear qualitative representation of the underlying phase-space structures over the timescales of interest. Furthermore, these state-of-the-art tools can be used to treat both geocentric and selenocentric orbits (governed by the perturbed two-body problem) and libration-point orbits (governed by the restricted three-body problem) in a more holistic framework.

We first use the fast-Lyapunov indicator (FLI) to detect the location and structure of very strong chaos in the cislunar space environment and to identify instabilities that act rather quickly (on the timescale of orbital periods). The fiducial simulations are set up such that the mean anomaly M of the TPs are initially 60° ahead of or behind the Moon in its orbit, and such that their initial inclination i, argument of perihelion ω, and longitude of ascending node Ω are equal to those of the Moon at a particular epoch. In this way, we mapped the dynamics of TPs initially in the orbital plane of the Moon with an L_4- and L_5-Lagrange-point-like configurations, respectively.

Fig. 6 shows the result of this FLI analysis applied from xGEO to beyond the semi-major axis of L_2, for all elliptic eccentricities, and considering realistic N-body simulations. The FLI was computed over a 9-months integration for a large grid of initial semi-major axis a and eccentricity e, for fixed initial (i,ω,Ω,M), and represented by a color scale, where lighter regions correspond to chaotic orbits and darker colors represent stable zones (on the considered

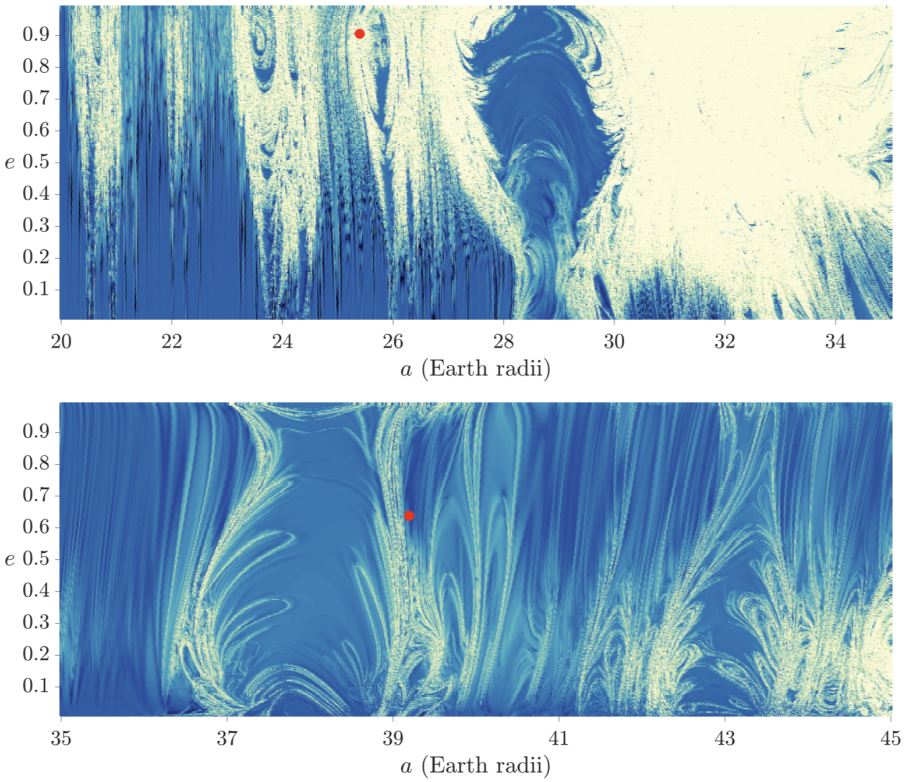

Fig. 7: MEGNO maps of the cislunar regions near IBEX and TESS, adopting a dynamical model in `REBOUND` that contains the Sun and Moon as perturbers. The map samples over a dense grid of initial values of (a, e), where the initial inclination i, argument of perihelion ω, longitude of ascending node Ω, and mean anomaly M are set equal to that of the orbits of IBEX (*top*) and TESS (*bottom*). Stable orbits appear with a *darker* color, while *lighter* regions correspond to chaotic orbits. The locations of IBEX and TESS are given by the *red dot*.

timescale). In all maps, rich foliated structures emerge interior to L_1 and exterior to L_2. Note that such maps cover a much broader range of three-body energies than previously treated, which, hitherto, have largely been limited to the bottlenecks near L_1 and L_2. These global space-manifold maps also reveal that while the inclusion of the Sun does not qualitatively disrupt the structures, it induces important quantitative differences that cannot be ignored for SSA. Averaging such maps over all orbital phases will also provide a framework to represent the dynamical sensitivity of various regimes in terms of the most intuitive parameters (i.e., orbital elements), and can be used to identify relevant metrics for surveillance design strategies (e.g., search and revisit rates, accuracy, surveillance volume).

These robust stability metrics, when computed over longer (decadal) timescales, can also be used to locate the orbital resonances that significantly affect the global structure of phase space. As an example of how such global-stability approaches can aid in mission analysis and design and cislunar SSA (e.g., space-based surveillance [77]), consider NASA IBEX's satellite. As described earlier in §1, IBEX's nominal orbit turned out to be chaotic and unpredictable as a result of significant lunar perturbations, and IBEX was subsequently placed in a novel resonant orbit with the Moon that is stable to this day [51]. Fig. 7 shows that an a priori analysis of the phase space, as permitted by MEGNO, would not only ensure that missions have predictable behaviors over the nominal (and possibly extended) scenario, thus avoiding an IBEX-like situation, but that such spacecraft can safely meet their demise through Earth reentry (without the need to make future significant orbital adjustments á la ESA's INTEGRAL mission [55]). The precarious state of IBEX's nominal operational orbit, perched on the threshold of chaos, is clearly revealed by Fig. 7 (*top panel*). A full understanding of the nature and consequences of the chaos in these environments would have certainly helped in the early design phases of the mission. Such knowledge was partially used in the design of TESS's orbit [58], located in Fig. 7 (*bottom panel*) in a narrow strip of stability; however, there remain many unresolved issues with our understanding of lunar MMRs, on which future numerical and theoretical research will help shed needed light.

4. CISLUNAR SPACE SUSTAINABILITY

Cislunar space, outside the confines of near-Earth satellite orbits, is poised to serve as a new high ground for space operations, and, like its circumterrestrial counterpart, must be sustained against risk from debris and other threats [78]. It is precisely the distinctive and multi-faceted dynamical features of this regime that complicates SSA efforts and represents significant challenges for space sustainability [1, 12–17, 78]. While end-of-life (EOL) disposal options are well established for missions in LEO (atmospheric decay) and GEO (near circular graveyards), existing mitigation guidelines do not fully regulate the whole, usable cislunar orbital space, including the very distant, highly eccentricity orbits (HEOs) of science missions.

Explorer VI (1959 Delta 1), with an apogee of 48 700 km, perigee of 6649 km, and equatorial inclination of 47°, represented the first satellite to be deliberately launched into a HEO, prompting the first detailed studies of the perturbing gravitational forces of the Sun and Moon acting on near-Earth satellites. The effects of these distant third bodies were often assumed negligible in comparison to the perturbing forces due to the Earth's oblateness, but in the case of HEOs, were found to change the elements of the orbit to a large degree over extended periods of time. Kozai found that lunisolar perturbations shortened the orbital lifetime of Explorer VI by a factor of ten, and Musen et al. found that it could be as little as a month, depending on the time of day of launch [79]. These results became significant in deciding the launch programs for future satellites with highly eccentric orbits, and the term 'launch window', originally applied to lunar and interplanetary probes to designate minimum-energy missions, was adapted to Earth-satellite missions to indicate when all orbital constraints will be satisfied [80, 81]. Explorer XII (1961 Upsilon) was the first satellite to be launched at a time that was preselected for a minimum orbital lifetime of a year, utilizing lunisolar perturbations to ensure relative stability [82].

For these science missions, the time of launch, and therefore the location of the orbit in space, must be chosen to satisfy a number of limiting constraints. The orbital launch window restraints, imposed by the satellite and experiments, generally entail that the perigee height will not drop below a certain value to minimize the radiation dose and that the orbital lifetime exceeds the nominal mission time; that the eclipse duration is limited and to spend several hours in sunlight between injection and the first eclipse; that the angle between the line of apsides and Earth-Sun line be fixed or other experimental constraints; and to maximize the science collection time and maintain communications. In all of existing launch window studies, the orbital lifetime is a factor, but its reduction or control is hardly a consideration.

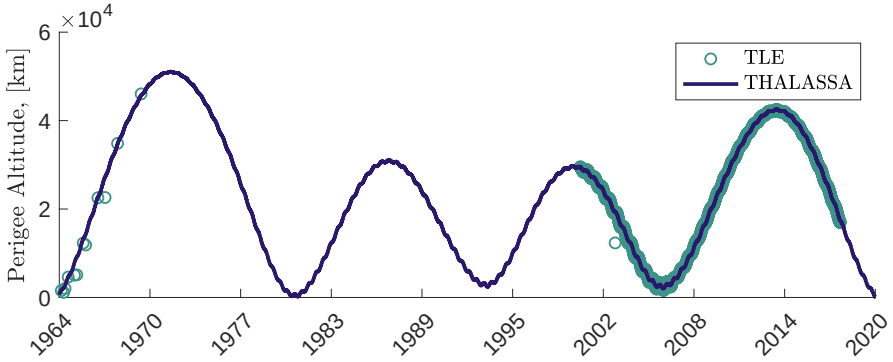

Fig. 8: Predicted perigee height (closest approach) of NASA's Orbiting Geophysical Observatory [80] (1964-054A) obtained using `THALASSA`, compared to TLEs [43]. This satellite was launched in 1964 into a very distant, elongated orbit, making tracking and prediction extremely challenging. Accordingly, 30 years of TLE data is missing from the public catalog.

Fig. 8 shows the recovered decadal trajectory of the NASA Orbiting Geophysical Observatory (EGO; satellite no. 1964-054A), previously mentioned in §1. In this case, the TLE data was missing for a span of 30 years after which tracking was resumed. We adopted a new dynamically-inclined route to orbit prediction based on TLEs to obtain statistically accurate initial conditions for the long-term propagation of orbits [43]. This method is implemented in Fig. 8 to recover the full multi-decadal trajectory of EGO (1964-054A), whose orbital lifetime was dramatically mispredicted in the late 1960's [52, 80, 81]. Fig. 9 shows both the historical launch window [80] with new lifetime

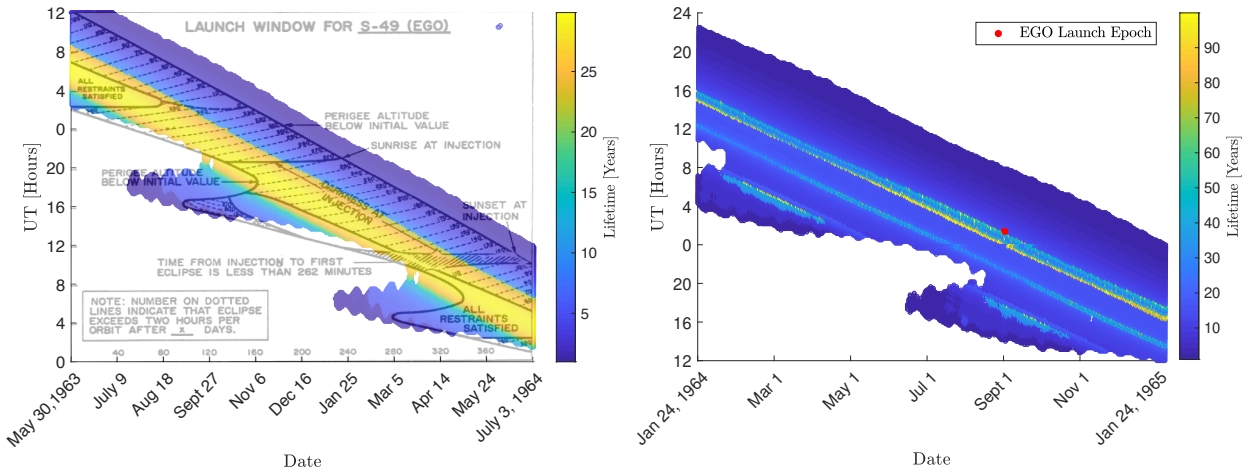

Fig. 9: Lifetime map of the nominal EGO launch conditions superimposed onto the historic launch window created by Montgomery [80] (*left*). Placement of the actual EGO launch epoch onto the lifetime map created using "corrected" launch conditions (*right*).

maps superimposed, showing that EGO lied on the cusp of the longest lifetime orbits for its actual launch conditions. While the LEO-to-GEO crossing orbit of EGO finally met its demise in August 2020, had the launch been delayed or advanced by just ten minutes, it would have re-entered decades ago, without otherwise compromising the mission. Such detailed a priori analyses and forethought [78] should become a major consideration for operational planning in the highly sensitive dynamical environment of xGEO space so that we may avoid the unfettered debris growth that plagues our traditional geocentric domains [83].

5. CONCLUSIONS AND OUTLOOK

While the capability of the U.S. to maintain space situational and domain awareness in the confines of the traditional orbits out to the geosynchronous belt is mature, the extreme range, the totality of relevant orbits, difficult observing geometries, and unstable astrodynamics create particular challenges associated with conducting SSA and SDA in the vast cislunar environment. In an SSA context, for example, both the modest stationkeeping for orbit maintenance in libration point trajectories, as demonstrated by the NASA ARTEMIS spacecrafts (Fig. 5), and the intrinsic sensitivity of these trajectories on account of space-manifold dynamics can serve to complicate attempts to maintain custody of an object in this unstable orbital environment. It is precisely these distinctive dynamical features, including rapid uncertainty propagation, that frustrate SSA but enable novel space-mission concepts that are not simply predicated by Keplerian motion.

We have used modern tools and techniques of Solar-System dynamics (e.g., stability indicators, fast and reliable *N*-body integrators) to probe the multi-timescale dynamics of xGEO space, showing how dynamical cartographies projected in the conical elements can be leveraged to characterize this largely unstable regime, which includes lunar MMRs and secular resonances that affect the orbital lifetimes of satellites and debris. Though a useful approach for obtaining a global picture of phase-space structure, the major drawback of both the FLI and MEGNO is that they require the simultaneous integration of the coupled system and variational equations. This renders them computationally taxing for use with an ephemeris formulation or for studying a hierarchy of simplified dynamical models, as is necessary for cislunar SSA. Future work will investigate other xGEO orbit parameterizations [84] as well as the use of a trajectory-based diagnostic known as the Lagrangian descriptors (LDs) [85], as suggested by Daquin and colleagues [86], to more thoroughly map out the six-dimensional phase-space dynamics and subsequently link this knowledge to processes that support the ground- and space-based surveillance and maintenance of a cislunar SOC [2, 87]. In addition to cislunar SSA, these insights could also reveal new options for trajectory design and spacecraft disposal that, up to now, have been obscured by the complexities introduced by higher fidelity models or detailed investigations into isolated parts of a missions' orbital phase space.

ACKNOWLEDGEMENTS

Some aspects of this work were done in collaboration with D. Amato, R. Malhotra, H. Namazyfard, S. D. Ross, and D. Wu. I am especially indebted to K. Parsay (NASA GSFC) and J. Spurbeck (Maxar Technologies) for many fruitful discussions on `GMAT` and the ARTEMIS trajectories, V. Mallik (Planet Labs) for insightful conversations on uncertainty propagation, and to the others for providing several useful figures. This material is based upon work supported by the Air Force Office of Scientific Research under Grant No. FA9550-21-1-0191.

6. REFERENCES

[1] M. J. Holzinger, C. C. Chow, and P. Garretson. A Primer on Cislunar Space. Technical Report 2021-1271, AFRL, 2021.

[2] M. Bolden, T. Craychee, and E. Griggs. An evaluation of observing constellation orbit stability, low signal-to-noise, and the too-short-arc challenges in the cislunar domain. In *Advanced Maui Optical and Space Surveillance Technologies Conference (AMOS)*, Maui, HI, 2020.

[3] A. J. Rosengren, D. K. Skoulidou, K. Tsiganis, and G. Voyatzis. Dynamical cartography of Earth satellite orbits. *Advances in Space Research*, 63:443–460, 2019.

[4] F. Gachet, A. Celletti, G. Pucacco, and C. Efthymiopoulos. Geostationary secular dynamics revisited: Application to high area-to-mass ratio objects. *Celestial Mechanics and Dynamical Astronomy*, 128:149–181, 2017.

[5] T. Nie and P. Gurfil. Lunar frozen orbits revisited. *Celestial Mechanics and Dynamical Astronomy*, 130:61 (35 pp.), 2018.

[6] M. Lara. *Hamiltonian Perturbation Solutions for Spacecraft Orbit Prediction: The Method of Lie Transforms*. De Gruyter, Berlin, 2021.

[7] W. S. Koon, M. W. Lo, J. E. Marsden, and S. D. Ross. *Dynamical Systems, the Three-Body Problem and Space Mission Design*. Springer-Verlag, New York, 2006.

[8] J. S. Parker and R. L. Anderson. *Low-energy Lunar Trajectory Design*. Wiley, Hoboken, 2014.

[9] A. J. Schwaniger. Trajectories in the Earth-Moon Space with Symmetrical Free-Return Properties. Technical Report TN D-1833, NASA, 1963.

[10] V. A. Egorov. *Three-Dimensional Lunar Trajectories*. Israel Program for Scientific Translations, Jerusalem, 1969.

[11] R. W. Farquhar and A. A. Kamel. Quasi-periodic orbits about the translunar libration point. *Celestial Mechanics*, 7:458–473, 1973.

[12] E. M. Zimovan-Spreen and K. C. Howell. Dynamical structures nearby NRHOs with applications in cislunar space. In *Proceedings of the AAS/AIAA Space Flight Mechanics Meeting*, Ka'anapali, Maui, HI, Paper AAS 19-808, 2019.

[13] E. E. Fowler, S. B. Hurtt, and D. A. Paley. Observability metrics for space-based cislunar domain awareness. In *Proceedings of the AAS/AIAA Space Flight Mechanics Meeting*, Orlando, FL, Paper AAS 20-575, 2020.

[14] J. K. Vendl and M. J. Holzinger. Cislunar periodic orbit analysis for persistent space object detection capability. In *Proceedings of the AAS/AIAA Space Flight Mechanics Meeting*, Orlando, FL, Paper AAS 20-487, 2020.

[15] C. Channing Chow, C. J. Wetterer, K. Hill, et al. Cislunar periodic orbit families and expected observational features. In *Advanced Maui Optical and Space Surveillance Technologies Conference (AMOS)*, Maui, HI, 2020.

[16] J. Ren, M. Li, and J. Zheng. Families of transfers from the Moon to distant retrograde orbits in cislunar space. *Astrophysics and Space Science*, 365:192 (21 pp), 2020.

[17] C. Frueh, K. Howell, K. J. DeMars, and S. Bhadauria. Cislunar space situational awareness. In *Proceedings of the AAS/AIAA Space Flight Mechanics Meeting*, Virtual, Paper AAS 21-290, 2021.

[18] A. J. Rosengren and D. J. Scheeres. Cis-lunar trajectories. In B. Cudnik, editor, *Encyclopedia of Lunar Science*, page In Press. Springer, Cham, 2021.

[19] M. Belló, G. Gómez, and J. J. Masdemont. Invariant manifolds, Lagrangian trajectories and space mission design. In E. Perozzi and S. Ferraz-Mello, editors, *Space Manifold Dynamics: Novel Spaceways for Science and Exploration*, pages 1–96. Springer, New York, 2010.

[20] Gómez, W. S. G., Koon, M. W. Lo, J. E. Marsden, J. Masdemont, and S. D. Ross. Connecting orbits and invariant manifolds in the spatial restricted three-body problem. *Nonlinearity*, 17:1571–1606, 2004.

[21] K. K. Boudad, K. C. Howell, and D. C. Davis. Dynamics of synodic resonant near rectilinear halo orbits in the bi-circular four-body problem. *Advances in Space Research*, 66:2194–2214, 2020.

[22] J. T. Fitzgerald and S. D. Ross. Theory of low-energy transit orbits in the periodically-perturbed restricted three-body problem. In *Proceedings of the AAS/AIAA Space Flight Mechanics Meeting*, Virtual, Paper AAS 21-317, 2021.

[23] C. J. Scott and D. B. Spencer. Calculating transfer families to periodic distant retrograde orbits using differential correction. *Journal of Guidance, Control, and Dynamics*, 33:1592–1605, 2010.

[24] M. Stramacchia, C. Colombo, and F. Bernelli-Zazzera. Distant retrograde orbits for space-based near earth objects detection. *Advances in Space Research*, 58:967–988, 2016.

[25] C. Bezrouk and J. S. Parker. Long term evolution of distant retrograde orbits in the Earth-Moon system. *Astrophysics and Space Science*, 362:176 (11 pp), 2017.

[26] R. Jedicke, B. T. Bolin, and W. F. Bottke. Earth's minimoons: Opportunities for science and technology. *Frontiers in Astronomy and Space Sciences*, 5:13 (19 pp.), 2018.

[27] M. Lara. Design of distant retrograde orbits based on a higher order analytical solution. *Acta Astronautica*, 161: 562–578, 2019.

[28] P. Pires and O. C. Winter. Location and stability of distant retrograde orbits around the Moon. *Monthly Notices of the Royal Astronomical Society*, 492:2727–2735, 2020.

[29] R. Zhang, Y. Wang, H. Zhang, and C. Zhang. Transfers from distant retrograde orbits to low lunar orbits. *Celestial Mechanics and Dynamical Astronomy*, 132:41 (30 pp), 2018.

[30] K. C. Howell and J. V. Breakwell. Almost rectilinear halo orbits. *Celestial Mechanics*, 32:29–52, 1984.

[31] D. García Yárnoz, J. P. Sanchez, and C. R. McInnes. Easily retrievable objects among the neo population. *Celestial Mechanics and Dynamical Astronomy*, 116:367–388, 2013.

[32] K. Oshima. The use of vertical instability of l1 and l2 planar lyapunov orbits for transfers from near rectilinear halo orbits to planar distant retrograde orbits in the Earth-Moon system. *Celestial Mechanics and Dynamical Astronomy*, 131:14 (28 pp), 2019.

[33] H. Chen, J. Liu, L. Long, et al. Lunar far side positioning enabled by a CubeSat system deployed in an Earth-Moon halo orbit. *Advances in Space Research*, 64:28–41, 2019.

[34] S. Trofimov, M. Shirobokov, A. Tselousova, and M. Ovchinnikov. Transfers from near-rectilinear halo orbits to low-perilune orbits and the Moon's surface. *Acta Astronautica*, 167:260–271, 2020.

[35] E. M. Zimovan-Spreen, K. C. Howell, and D. C. Davis. Near rectilinear halo orbits and nearby higher-period dynamical structures: orbital stability and resonance properties. *Celestial Mechanics and Dynamical Astronomy*, 132:28 (25 pp), 2020.

[36] M. Bolliger, M. R. Thompson, et al. Ground-based navigation trades for operations in Gateway's near rectilinear halo orbit. In *Proceedings of the AAS/AIAA Space Flight Mechanics Meeting*, Virtual, Paper AAS 21-450, 2021.

[37] D. Conte, M. Di Carlo, K. Ho, et al. Earth-Mars transfers through Moon distant retrograde orbits. *Acta Astronautica*, 143:372–379, 2018.

[38] D. D. Mazanek, D. M. Reeves, P. A. Abell, et al. Asteroid Redirect Mission (ARM) Formulation. Assessment and Support Team (FAST) Final Report. Technical Report NASA/TM 2016-219011, NASA STI Program, 2016.

[39] E. Perozzi, M. Ceccaroni, G. B. Valsecchi, and A. Rossi. Distant retrograde orbits and the asteroid hazard. *The European Physics Journal Plus*, 132:367 (9 pp), 2017.

[40] D. Chongrui, M. K. Fain, and O. L. Starinova. Analysis and design of halo orbits in cislunar space. *IOP Conference Series: Materials Science and Engineering*, 984:012033 (11 pp), 2020.

[41] S. Yun, K. Tuggle, R. Zanetti, and C. D'Souza. Sensor configuration trade study for navigation in near rectilinear halo orbits. *The Journal of the Astronautical Sciences*, 67:1755–1774, 2020.

[42] N. H. Crisp, K. Smith, and P. Hollingsworth. Launch and deployment of distributed small satellite systems. *Acta Astronautica*, 114:65–78, 2015.

[43] H. Namazyfard, A. J. Rosengren, D. Amato, C. Bombardelli, and L. Dell'Elce. Accurate recovery of ephemerides from TLEs of resonant orbits. In *Key Topics in Orbit Propagation Applied to Space Situational Awareness*, Logroño, Spain, 2019.

[44] A. J. Rosengren, H. Namazyfard, and G.E.O. Giacaglia. Effects of higher-order multipoles of the lunar disturbing potential on elongated orbits in cislunar space. *European Physics Journal Special Topics*, 229:1545–1555, 2020.

[45] D. Amato, R. Malhotra, V. Sidorenko, and A. J. Rosengren. Lunar close encounters compete with the circumterrestrial Lidov–Kozai effect: The dynamical demise of Luna 3. *Celestial Mechanics and Dynamical Astronomy*, 132:35 (18 pp), 2020.

[46] G. H. Ludwig. The orbiting geophysical observatories. *Space Science Reviews*, 2:175–218, 1963.

[47] P. Butler. Interplanetary monitoring platform, 1980. NASA-TM-80758.

[48] A.A. Galeev, Yu. I. Gal'Perin, and L.M. Zelenyi. The INTERBALL-1 project to study solar-terrestrial physics. *Kosmicheskie Issledovaniia*, 34:339–362, 1996.

[49] F. Jansen, D. Lumb, B. Altieri, et al. XMM-Newton observatory: I. The spacecraft and operations. *Astronomy and Astrophysics*, 365:L1–L6, 2001.

[50] N. A. Eismont, A. V. Ditrikh, G. Janin, et al. Orbit design for launching INTEGRAL on the Proton/Block-DM launcher. *Astronomy and Astrophysics*, 411:L37–L41, 2003.

[51] D. J. McComas, J. P Carrico, Jr., B. Hautamaki, et al. A new class of long-term stable lunar resonance orbits: Space weather applications and the Interstellar Boundary Explorer. *Space Weather*, 9, 2011. S11002 (9 pp.).

[52] B. E. Shute and J. Chiville. The lunar-solar effect on the orbital lifetimes of artificial satellites with highly eccentric orbits. *Planetary and Space Science*, 14:361–369, 1966.

[53] G. Janin and E. A. Roth. Decay of a highly eccentric satellite. *Celestial Mechanics*, 14:141–149, 1976.

[54] J.J.F. Liu, J. Segrest, and V. Szebehely. Orbit mechanics of deep space probes. *The Journal of the Astronautical Sciences*, 34:171–187, 1986.

[55] R. Armellin, J. F. San-Juan, and M. Lara. End-of-life disposal of high elliptical orbit missions: The case of INTEGRAL. *Advances in Space Research*, 56:479–493, 2015.

[56] V. T. Gontkovskaya and G. A. Chebotarev. Lunar and solar perturbations of lunik iii. *Soviet Astronomy*, 5: 728–732, 1962.

[57] D. J. Dichmann, R. Lebois, and J. P. Carrico, Jr. Dynamics of orbits near 3:1 resonance in the Earth-Moon system. *The Journal of the Astronautical Sciences*, 60:51–86, 2014.

[58] G. R. Ricker, J. N. Winn, R. Vanderspek, et al. Transiting exoplanet survey satellite. *Journal of Astronomical Telescopes, Instruments, and Systems*, 1:014003 (10 pp.), 2015.

[59] J. N. Winn and D. C. Fabrycky. The occurrence and architecture of exoplanetary systems. *Annual Review of Astronomy and Astrophysics*, 53:409–447, 2015.

[60] K. Batygin and M. E. Brown. Evidence for a distant giant planet in the solar system. *The Astrophysical Journal*, 151:22 (12pp), 2016.

[61] X. Wang and R. Malhotra. Mean motion resonances at high eccentricities: The 2:1 and 3:2 interior resonances. *The Astronomical Journal*, 154:20 (12pp), 2017.

[62] N. Todorović, D. Wu, and A. J. Rosengren. The arches of chaos in the Solar System. *Science Advances*, 6: eabd1313, 2020.

[63] D. C. Davis, S. M. Phillips, and B. P. McCarthy. Trajectory design for saturnian ocean worlds orbiters using multidimensional poincaré maps. *Acta Astronautica*, 143:16–28, 2018.

[64] B. D. Anderson, M. W. Lo, and M. Vaquero. The stability of orbital resonances for europa quarantine design: escape orbit case. In *Proceedings of the AAS/AIAA Space Flight Mechanics Meeting*, Ka'anapali, Maui, Paper AAS 19-481, 2019.

[65] R. L. Anderson. Tour design using resonant-orbit invariant manifolds in patched circular restricted three-body problems. *Journal of Guidance, Control, and Dynamics*, 44:106–119, 2021.

[66] Ch. Skokos. The Lyapunov characteristic exponents and their computation. *Lecture Notes in Physics*, 790: 63–135, 2010.

[67] H. Rein and D. S. Spiegel. Ias15: a fast, adaptive, high-order integrator for gravitational dynamics, accurate to machine precision over a billion orbits. *Monthly Notices of the Royal Astronomical Society*, 2:1424–1437, 2015.

[68] H. Rein, D. M. Hernandez, and D. Tamayo. Hybrid symplectic integrators for planetary dynamics. *Monthly Notices of the Royal Astronomical Society*, 485:5490–5497, 2019.

[69] H. Rein and S. F. Liu. Rebound: an open-source multi-purpose n-body code for collisional dynamics. *Astronomy and Astrophysics*, 537:A128 (10 pp), 2015.

[70] D. Amato, C. Bombardelli, G. Baú, V. Morand, and A. J. Rosengren. Non-averaged regularized formulations as an alternative to semi-analytical orbit propagation methods. *Celestial Mechanics and Dynamical Astronomy*, 131:21 (38 pp.), 2019.

[71] T. H. Sweetser, S. B. Broschart, V. Angelopoulos, et al. ARTEMIS mission design. *Space Science Reviews*, 165: 27–57, 2011.

[72] V. T. Gontkovskaya and G. A. Chebotarev. The motion of the space probe lunik iii. *Soviet Astronomy*, 5:91–94, 1961.

[73] F. R. Hoots. SGP4-XP A New TLE Orbit Prediction Model. Technical Report TOR-2021-00780, Aerospace, 2021.

[74] E. Lega, M. Guzzo, and C. Froeschlé. Theory and applications of the fast lyapunov indicator (FLI) method. In Ch. Skokos, G. A. Gottwald, and J. Laskar, editors, *Chaos Detection and Predictability*, pages 35–54. Springer, Berlin, Heidelberg, 2016.

[75] P. Cincotta, C. Giordano, and C. Simó. Phase space structure of multi-dimensional systems by means of the mean exponential growth factor of nearby orbits. *Physica D*, 182:151–178, 2003.

[76] N. Nakhjiri and B. F. Villac. Automated stable region generation, detection, and representation for applications to mission design. *Celestial Mechanics and Dynamical Astronomy*, 123:63–83, 2015.

[77] P. M. Cunio, M. J. Bever, and B. R. Flewelling. Payload and constellation design for a solar exclusion-avoiding cislunar SSA fleet. In *Advanced Maui Optical and Space Surveillance Technologies Conference (AMOS)*, Maui, HI, 2020.

[78] N. R. Boone and R. A. Bettinger. Cislunar debris propagation following a catastrophic spacecraft mishap. In *Proceedings of the AAS/AIAA Space Flight Mechanics Meeting*, Virtual, Paper AIAA 2021-0102, 2021.

[79] E. Upton, A. Bailie, and P. Musen. Lunar and solar perturbations on satellite orbits. *Science*, 130:1710–1711, 1959.

[80] H. E. Montgomery. EGO Launch Window Study. Technical Report TM-X-55413, NASA, 1963.

[81] B. E. Shute. Prelaunch Analysis of High Eccentricity Orbits. Technical Report TN-D-2530, NASA, 1964.

[82] R. J. Sandifer and B. E. Shute. Effect of solar-lunar perturbations on the lifetime of Explorer XII (abstract). *The Astronomical Journal*, 67:282, 1962.

[83] A. Witze. The quest to conquer Earth's space junk problem. *Nature*, 24:25–26, 2018.

[84] A. Peloni, C. R. McInnes, and M. Ceriotti. Osculating Keplerian elements for highly non-Keplerian orbits. *Journal of Guidance, Control, and Dynamics*, 41:2486–2495, 2018.

[85] C. Lopesino, F. Balibrea-Iniesta, V. J. García-Garrido, S. Wiggins, and A. M. Mancho. A theoretical framework for Lagrangian descriptors. *International Journal of Bifurcation and Chaos*, 27:1730001 (25 pp.), 2017.

[86] R. Pedenon-Orlanducci, T. Carletti, and J. Daquin. Geometric parametrisation of Lagrangian Descriptors for 1 degree-of-freedom systems. In *2nd Online Conference on Nonlinear Dynamics and Complexity*, Virtual, 2021.

[87] P. Dao, K. Haynes, V. Frey, et al. Simulated photometry of objects in cislunar orbits. In *Advanced Maui Optical and Space Surveillance Technologies Conference (AMOS)*, Maui, HI, 2020.